Direct Fusion Drive Rocket for Asteroid Deflection

IEPC-2013-296

Presented at the 33rd International Electric Propulsion Conference,
The George Washington University, Washington, D.C., USA
October 6–10, 2013

Joseph B. Mueller* and Yosef S. Razin† and Michael A. Paluszek ‡ and Amanda J. Knutson § and Gary Pajer ¶
Princeton Satellite Systems, 6 Market St, Suite 926, Plainsboro, NJ, 08536, USA

Samuel A. Cohen‖
Plasma Physics Laboratory, 100 Stellarator Road, Princeton, NJ, 08540

and

Allan H. Glasser**
University of Washington, Department of Aeronautics and Astronautics, Guggenheim Hall, Seattle, WA 98195

Traditional thinking presumes that planetary defense is only achievable with years of warning, so that a mission can launch in time to deflect the asteroid. However, the danger posed by hard-to-detect small meteors was dramatically demonstrated by the 20 meter Chelyabinsk meteor that exploded over Russia in 2013 with the force of 440 kilotons of TNT. A 5-MW Direct Fusion Drive (DFD) engine allows rockets to rapidly reach threatening asteroids that and deflect them using clean burning deuterium-helium-3 fuel, a compact field-reversed configuration, and heated by odd-parity rotating magnetic fields. This paper presents the latest development of the DFD rocket engine based on recent simulations and experiments as well as calculations for an asteroid deflection envelope and a mission plan to deflect an Apophis-type asteroid given just one year of warning. Armed with this new defense technology, we will finally have achieved a vital capability for ensuring our planet's safety from impact threats.

*Senior Technical Staff, jmueller@psatellite.com.
†Technical Staff, yrazin@psatellite.com.
‡President, mpaluszek@psatellite.com.
§Senior Technical Staff, aknutson@psatellite.com.
¶Senior Scientist, gpajer@psatellite.com.
‖Director of the Program in Plasma Science & Technology, scohen@pppl.gov
**Research Scientist, ahg5@uw.edu.

Nomenclature

a = Acceleration
b = Distance of closest earth approach
D = Deuterium
f_p = Neutron production fraction
He = Helium 3
H = Hydrogen
Q = Fusion power gain
m = Mass
m_A = Asteroid mass
m_S = Time varying part of the spacecraft mass
t = Time
P = Power
T = Thrust
u_E = Exhaust velocity
u_k = Applied accelerations
Z = Atomic number
β = Ratio of magnetic pressure to plasma pressure
η = Fusion power to thrust conversion efficiency

1. Introduction

Asteroids pose a major threat to the earth;[1] therefore, many methods have been proposed for deflecting asteroids. These include vaporizing the asteroids with lasers or nuclear explosives, using a solar sail or e-sail,[2] imparting an immediate velocity change through high speed kinetic impact, changing the albedo of the asteroid such that its orbit is altered using solar pressure, using the gravitational attraction between the asteroid and the spacecraft,[3] focusing sunlight to burn a hole that enables passive propulsion from outgassing, and others. This paper explores the use of a rocket engine based on nuclear fusion to rendezvous with and move an asteroid. The engine is based on a 5 MW Direct Fusion Drive (DFD)[4–6] and is presented in the context of a conceptual spacecraft. The transfer orbit to the asteroid is developed along with the strategy for moving the asteroid. The benefit of using the DFD is that it can apply moderate variable thrust with high exhaust velocity, enabling it to reach asteroids more quickly and impart more delta-v than traditional propulsion methods.

The paper is organized as follows. We first provide an overview of the DFD design, with a brief discussion of the fundamental physics behind the technology. The reader is referred to previous publications[4–6] for a more in-depth presentation. We then examine the threats posed by asteroids of different size, considering their relative likelihood and risk. Next, we discuss the overall mission design. We begin by describing the spacecraft design and concept of operations, followed by a deflection maneuver strategy that is based on achieving a desired relative state in "b-plane" of the encounter. We then present an analysis of the deflection capability for an asteroid half the size of Apophis, and conclude with an example deflection maneuver.

2. Direct Fusion Drive Design

1. Overview

The Direct Fusion Drive (DFD) is comprised of multiple innovations that together yield a safer, more compact, and lighter-weight engine that directly produces a high exhaust velocity and medium thrust, and in addition produces electrical power. The field-reversed configuration (FRC) allows for magnetic confinement with a simpler, more natural geometry for propulsion than, for instance, a tokamak. The increased safety is due to the choice of an aneutronic fuel, D–^{3}He. The plasma is heated by an odd-parity rotating magnetic field ($\mathrm{RMF_o}$), which is predicted to promote better energy confinement, hence allow smaller, more stable engines. Other advantages include a small start-up system and a variable thrust propulsion system for more

flexible mission designs.

Much of the sub-systems and physics described below have been presented in more detail in Refs. 4–6.

2. FRC

The DFD design is based on on-going research with the Princeton FRC-2 (PFRC-2) and Magnetic Nozzle Experiment (MNX) at the Princeton Plasma Physics Laboratory. The PFRC-2 machine, the fourth prototype of six planned, is shown in Figure 1. In the PFRC, the plasma is shaped by the magnetic field, such that: a separatrix divides the closed-field region from the open-field region. Field-shaping coils that are magnetic flux conservers surround the plasma. Between the plasma and inner wall of the chamber is a scrape-off-layer, through which additional propellant can flow.

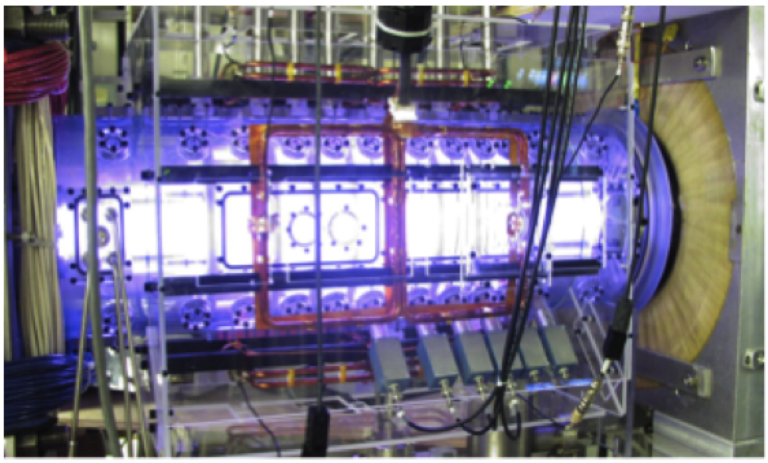

Figure 1. Plasma production in the PRFC-2

Figure 1 shows PFRC-2 under test at the Princeton Plasma Physics Laboratory. Testing of this machine will be complemented by a recently awarded research grant to study magnetic nozzles. The results of both experiments will guide the design of PFRC-3 that will be the last step before building a burning plasma machine.

3. Aneutronic D–^{3}He Fuel

The DFD is powered by burning D–^{3}He fuel, which only produces neutrons in some side reactions. Thus,

$$\mathrm{D} + {}^3\mathrm{He} \rightarrow {}^4\mathrm{He}\ (3.6\ \mathrm{MeV}) + \mathrm{p}\ (14.7\ \mathrm{MeV}) \quad (1)$$

$$\mathrm{D} + \mathrm{D} \rightarrow \mathrm{T}\ (1.01\ \mathrm{MeV}) + \mathrm{H}\ (3.02\ \mathrm{MeV}) \quad (2)$$

$$\mathrm{D} + \mathrm{D} \rightarrow {}^3\mathrm{He}\ (0.82\ \mathrm{MeV}) + \mathrm{n}\ (2.45\ \mathrm{MeV}) \quad (3)$$

where the values in parenthesis are the energy of that particular fusion product. Minimizing neutron production is crucial for space propulsion because it reduces the required shielding and consequently reduces the size, mass, and cost of the spacecraft. Additionally, the use of D–^{3}He increases the fraction of power available for propulsion by decreasing the energy and quantity of neutrons produced and completely eliminates the need to breed tritium (T), in contrast to reactions based on D–T.

There are a number of methods for further reducing the tritium and neutrons, as we have previously discussed including fine-tuning the stoichiometric ratio of the reactants and rapid tritium removal. Furthermore, our RF plasma heating method could reduce the fusion energy of D–D lost in neutrons from 33% to under 0.5%, by tailoring the ion energy distributions, based on work done by Cohen and Liu.[7]

4. The RMF$_o$ Heating Method

Beyond neutron reduction, the RMF$_o$ heating method was chosen because it allows for more stable confinement and a more compact reactor. For an FRC reactor to burn its D–^{3}He fuel mixture, the ^{3}He and D

average ion energies must achieve values of around 100 keV and 70 keV, respectively. Too large or dense an FRC is not well heated, such that an optimum FRC for RMF_o heating of ions to 100 keV and above has a radius in the range 20-30 cm. This places a lower limit on the confinement time required, no worse than a fifth of the benchmark classical value. Choosing the RMF_o's frequency and amplitude properly allows ions to be pumped up, repeatedly, to energies near the peak of the D–^{3}He fusion cross-section and then returned to the bulk temperature. This is a conservative process that increases the fusion rate and decreases neutron production, per Rider.[8]

Add to these effects that D–^{3}He fusion produces neutrons that have only one-sixth of the energy of those produced by burning D–T and the larger surface to volume ratio ($\propto$ 1/radius) for a small FRC compared to a large tokamak (20 cm *vs.* 10 m) and an additional 10,000-fold reduction of neutron power load on the wall is obtained. The shielding requirements for this type of small, clean reactor are far less than for a D–T fueled fusion engine.

The RMF_o method, in addition to reducing neutron production, also offers the possibility of a novel, direct energy extraction method from the fusion products. The same rotating azimuthal electric field that heats the ions can be used to extract energy from the 3.6 MeV alphas and 14.7 MeV protons produced by D–^{3}He fusion. Thus, RMF_o could provide both a high-efficiency way of extracting energy directly from the charged fusion products and maintain the center of mass ion energy for the D–^{3}He collision near the peak of its reactivity.[4]

5. Superconducting Flux Conservers

Radial confinement is achieved by the coaxial solenoidal field-shaping coil array, commonly termed flux conservers (FCs). FCs are superconducting rings, evenly spaced along the reactor length. The FCs in the PFRC-2 employ high-temperature superconducting materials set in a liquid nitrogen cooled copper mandrel. For a full discussion on the design, construction, and testing of the PFRC-2's FCs, see Myers.[9]

6. Reactor Chamber, Shielding, and Thermal Power Conversion

In designing the reactor chamber, some measures must be taken to promote fracture resistance and accommodate the dimensional alterations that occur given the production of some, even if minimal, neutron irradiation.[10] Therefore, the reactor chamber wall is composed of 20 cm of $^{10}B_4C$ neutron shielding, under one cm of tungsten for X-ray absorption, structural support, and a helium cooling blank. The Bremsstrahlung can be efficiently removed by flowing helium gas through $^{10}B_4C$ heat exchanger tubes containing corrugated sheets of refractory medium-Z material.[11] The Bremsstrahlung heats the high-Z materials to about 2000 K. With a thermal rejection temperature to space of 625 K, this results in a Carnot efficiency, η_C, of 69%.[12]

7. Magnetic Nozzle and Thrust Augmentation

The magnetic nozzle and thrust augmentation system allow directional control of the plasma and control of the thrust level and exhaust velocity. A magnetic nozzle, as described by Arefiev,[13] Tarditi,[14] and Cohen,[15] redirects the flow from the FRC to free space. Magnetic nozzles have been found to be highly efficient, especially with weakly magnetized propellants, with $\eta_{\text{plume}} > 85\%$.[16]

Thrust is increased by the addition of propellant, increasing mass flow and thrust at the expense of specific impulse.[17] A suitable propellant would be deuterium, which would be injected as a cold gas into the gas box and from there enter the open-field region. The gas would be ionized quickly, forming a plasma similar to what is called, in tokamak terminology, a high recycling divertor, or even a detached plasma. The cold plasma will flow around the outside of the separatrix with electrons picking up energy from the fusion products and synchrotron radiation as it passes through the OFR. Within the detached plasma regime, UEDGE simulations have shown efficiencies of at least η=0.8 for propellant flow from the gas box to the nozzle for our configuration.[18]

8. DFD Plasma Parameters

Plasma parameters were chosen by an iterative, self-consistent process. The selected fusion power density was based on an assumed plasma volume needed to produce the desired power. Then the plasma density and temperatures needed to produce that power density were selected to be consistent with both the estimated energy confinement time (1/5 of classical and radiation losses) and the magnetic field capabilities of current

high-temperature superconductors, incorporating a wide safety margin. The plasma radius was iterated at this point to provide a safety margin on the energy confinement. Further refinements in the plasma modeling were performed to reduce neutron wall load. These included increasing the ^{3}He/D ratio in the plasma and control of the detailed velocity distributions of the D and ^{3}He.

Many physics challenges remain before the RMF$_o$-heated FRC can be developed into a practical reactor. The predictions of excellent energy confinement, stability, efficient electron and ion heating, and current drive to fusion-relevant temperatures must be validated. Substantial progress has occurred in the first three areas. In 2010 and 2012, TriAlpha Energy Corp reported near-classical energy confinement time in their FRC.[19,20a] Our reactor needs energy confinement time only 1/5 as long as the classical. In 2007, an RMF$_o$ heated FRC[22] achieved stable plasma durations 3,000 times longer than predicted by MHD theory.[23] By 2012 that record was extended to over 10^5 times longer. Finally, theoretical studies by Glasser,[24] Landsman,[25] and Cohen[26] indicate that RMF$_o$ will be able to heat plasma electrons and ions to fusion relevant temperatures. These are promising starts, but much research is needed at higher plasma temperatures and densities and with burning, *i.e.*, fusing, plasmas.

Table 1. 5 MW fusion engine. Temperatures are approximations for a full non-Maxwellian particle distributions generated and sustained by the RMF$_o$. The majority of the available electrical power is returned to the RMF$_o$ to heat the plasma. The RF power generation mass is based on commercially available units from.[27]

Parameter	Value
β	0.85
Plasma radius	0.25 m
Plasma length	13.0 m
Axial magnetic field	4.8 T
Ion temperature	100.0 keV
e^- temperature	300.0 keV
Deuterium number density	5.3e+13 cm^{-3}
^{3}He number density	1.6e+14 cm^{-3}
e^- number density	3.7e+14 cm^{-3}
Masses	
Vacuum vessel mass	980 kg
Magnet mass	693 kg
RF power generation system mass	1050 kg
Heat rejection system mass	1013 kg
Thermal power conversion system mass	5790 kg
Shielding mass	19055 kg
Total engine mass	28581 kg
Power (Q $\approx$ 2)	
Fusion power	5.6 MW
RMF$_o$ power	2.5 MW
Bremsstrahlung power	1.3 MW
Synchrotron power	2.7 MW
Neutron power	2.59 kW
Waste heat	1.5 MW
Available electrical power	3.3 MW
Propulsion power	2.8 MW

[a]Classical confinement time occurs for Coulomb collision driven diffusion only. The confinement time of real plasma is often far less than the classical limit,.[21]

3. Asteroid Threats

Although early scientists suspected that comets and asteroids might be potentially dangerous, the transmission of images from exploratory interplanetary spacecraft of impact craters and scars on other planets in our solar system began to reveal clues about impact history on Earth.[28] Many large impact structures have been found on Earth, such as the Vredefort Crater in South Africa, the Sudbury Basin in Canada, the Chicxulub Crater in Mexico, and the Chesapeake Bay impact crater. The Chicxulub impact event temporally coincides with the K-T boundary and mass extinctions, leading many scientists to conclude that a similar event could cause global devastation in the future.[28] Near Earth Objects (NEOs) are classified as Potentially Hazardous Objects (PHOs) based on the minimum orbit interception distance. If the NEO passes close enough to the Earth, the potential for real impact may be unknown due to trajectory perturbations caused by close planetary flybys and limitations on integration accuracy over long simulation times.[28] Bodies identified as PHOs are more closely and carefully monitored until the impact risk is better understood.

Blast waves, fires, craters, earthquakes and tsunamis are all possible impact events.[29] Since the large extinction threatening impacts are statistically far less likely to occur and very small bodies are much less likely to cause damage on Earth, current disaster management focuses on intermediate sized NEOs ranging in diameter from a few tens of meters up to several kilometers. Bodies with diameters up to a few hundred meters are expected to cause blast damage, earthquakes, and fires which would create regional damage comparable to other recent natural disasters. NEOs with diameters up to one km would likely cause water vapor injections and ozone loss on a global scale. A two km diameter asteroid impact represents an approximate threshold between regional and global effects. Bodies sized at a few km would likely cause dust and sulfate levels high enough to interrupt photosynthesis cycles, and the reentering ejecta would set large scale fires. Events corresponding to bodies with diameters greater than 10 km would likely cause global effects that would result in mass extinction.[30]

The Torino scale, used to indicate the potential risk associated with an Earth orbit crossing a NEO, is both numbered and color coded to indicate the threat rating. Events that are likely to have no consequences are colored white and given a threat level of zero. Any event that merits careful consideration is colored green and labeled one. Events meriting concern are yellow and numbered two through four, and threatening events are colored orange and numbered five through seven. Certain collisions are colored red and number eight through ten depending on the devastation levels expected.[30]

1. Asteroid Rotation

Figure 2 gives rotation rates of Near Earth Objects. Spin rates are as high as 1000 revolutions per day.

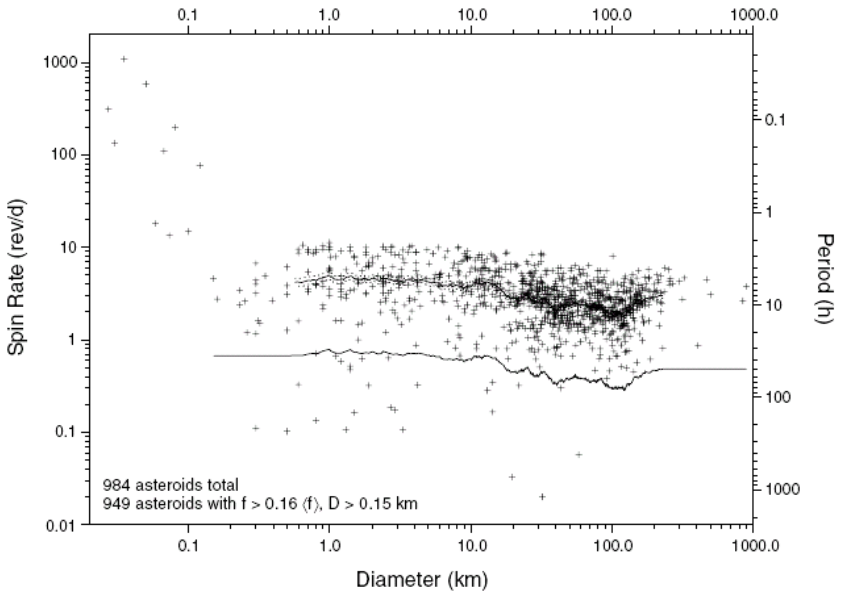

Figure 2. Rotation rates of near earth objects.[31]

Asteroid rotation presents a challenge to any method that applies a force to the asteroid. Asteroids that are rotating will not be in a simple spin. This means that the thruster can only be turned on when the thrust vector is aligned with the desired inertial direction. The gimbal mechanism descxribed above can partially alleviate this problem and potentially permits the application of a torque to slow the asteroid rotation rate while the thruster also applies a force. Further studies of asteroid rotation are required to see whether this is viable.

4. Mission Design

1. Asteroid Deflection Spacecraft

The asteroid deflection spacecraft is shown in Figure 3. The guidance, navigation and control system is discussed in reference 32, and the spacecraft is discussed in reference 5. The asteroid interface consists of three screws on a double gimbaled platform. The design is conceptual. The screws anchor the spacecraft onto the asteroid. The images show one screw partially deployed. The final design of the anchoring mechanism would depend on the nature of the asteroid material, and several types of anchors might be required.

The thrust vector direction is controlled by the gimbals and they can be used for attitude control of the asteroid/spacecraft combination. Because the DFD produces power along with thrust the gimbals can be high power and are not limited by the sun vector or asteroid shadowing of the sun.

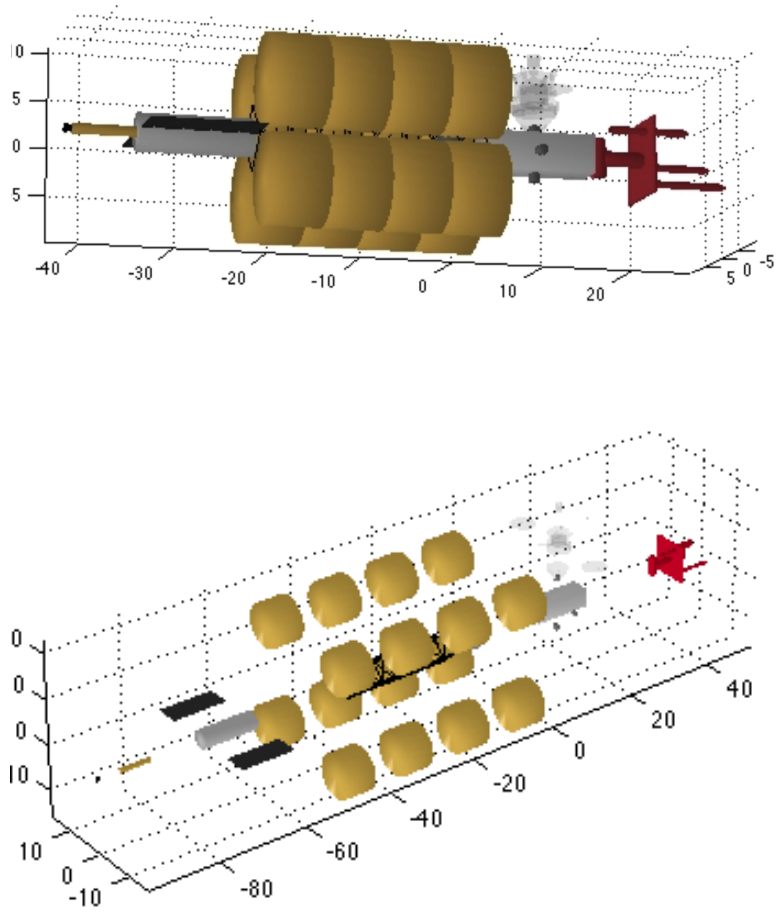

Figure 3. The Asteroid Deflection Spacecraft. The exploded view shows the central truss.

2. Concept of Operations

The spacecraft are based on a standard transfer vehicle for robotic missions. The spacecraft are maintained in low earth orbit at a DFD powered space station shown in Figure 4. They are used for a variety of missions and none are dedicated to asteroid deflection,which would be a very rare event.

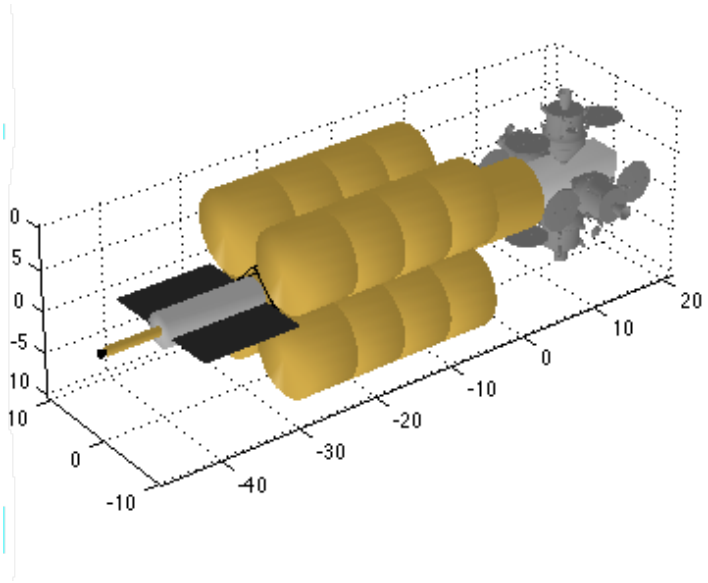

Figure 4. DFD powered space station.

Upon detection of an asteroid that has a high probability of hitting the earth, multiple transfer vehicles are configured with asteroid interface modules. It then spirals out of earth orbit and heads to the asteroid. Upon reaching the asteroid it lands on the asteroid and attaches using its interface module. The initial landing point is based on an estimate of the asteroid center-of-mass. A test burn is conducted and estimates made of the location of the asteroid center-of-mass is refined. The vehicle will then either reorient or possibly move to a new location. The idea is to have the engine fire through the asteroid center-of-mass along the desired velocity change direction.

3. Transfer to the Asteroid

Transfer is achieved using a modified Lambert law. Lambert's law assumes impulsive changes in velocity. With the modified Lambert's law we burn at a constant acceleration for several days both at the departure point and intercept point. This has little effect on the total required velocity change. The following plot displays the required ΔV to transfer to Apophis for a number of times of flight given an Earth departure date of April 13, 2027; two years prior to the 2029 close approach. This date is selected to allow time to transfer to the asteroid and perform the one year deflection maneuver.

The cost drops to less than 10 km/s and levels off once the time of flight surpasses 270 days. Although the transfer cost of reaching the asteroid is higher for shorter times of flight, the earlier arrival will afford more time to maneuver and will therefore require less Delta-v to perform the deflection. Maneuver deflection maneuvers are studied in the next section.

4. Competing Approaches to Asteroid Deflection

Asteroid deflection has been studied extensively.[33] Several methods have been proposed, but most can be placed into one of two categories: 1) instant kinetic impact or 2) perpetual thrust. In the former case, the asteroid velocity is changed due to the momentum transfer from a high relative velocity impact with the sacrificial spacecraft. In the latter case, the spacecraft acts as a tug boat of sorts, imparting an acceleration on the asteroid over time to gradually change its velocity. The kinetic impactor approach, while arguably simple in its conception, actually imposes significant complexity on the spacecraft design. Since the spacecraft mass is so much smaller than that of the asteroid, a correspondingly large relative velocity is necessary in order

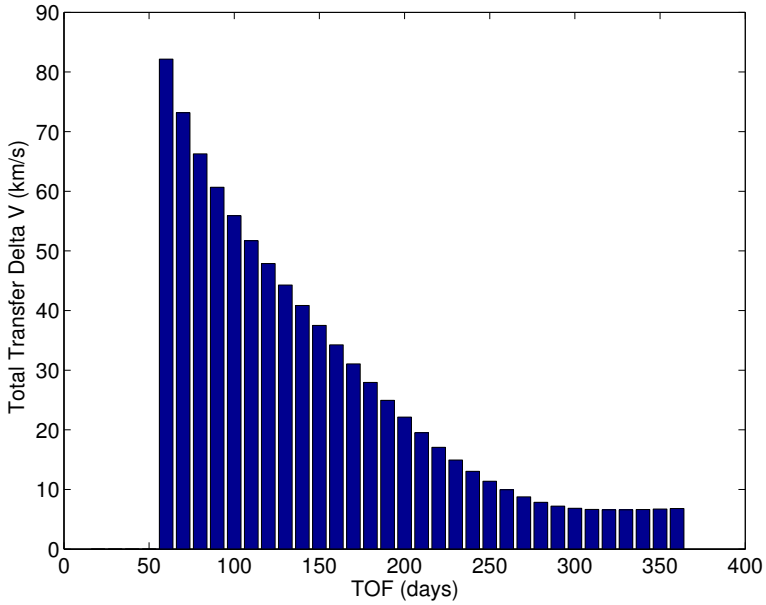

Figure 5. Delta v requirement as a function of TOF to transfer to Apophis given a departure date of April 13, 2027, two years prior to the near Earth pass.

to impart a significant momentum transfer. Furthermore, the spacecraft would have to impact very near to the center of mass of the asteroid. This presents an enormous challenge for the navigation and guidance systems, as it would have to accurately strike the asteroid while closing at extremely high speed, e.g. 30-60 km/s.

In this analysis, we consider the tug-boat method, where the spacecraft applies thrust over an extended period of time by anchoring itself to the asteroid. The goal is to gradually nudge the asteroid orbit over time so that we create the maximum separation distance (in some desired direction) at the predicted encounter time. Note that for the encounter, we want to avoid both a collision with Earth *now* as well as a future collision during the next encounter. In practice, Monte Carlo simulations are conducted to compute a region called a keyhole; if the asteroid passes through the keyhole then there is a high probability of a collision in the next encounter.

5. Encounter Geometry

A diagram of the encounter geometry is shown in Figure 6. This illustration of the asteroid trajectory is shown in an Earth-centered coordinate system. We follow the traditional approach for modeling the encounter, where the original unperturbed asteroid trajectory (not perturbed by Earth's gravity) approaches Earth along an asymptotic line. The direction of this line is simply the relative velocity of the asteroid with respect to Earth in the inertial heliocentric frame. The predicted closest point of approach occurs at distance b from Earth's center. The vector from Earth to the closest point of approach is called the "b-vector". The so-called "b-plane" contains the b-vector and is perpendicular to the incoming asymptote.

We now consider the 2029 encounter of Apophis with Earth, using the latest ephemeris from JPL Horizons. A plot of the b-plane encounter is shown in Figure 7. This agrees closely with the b-plane plot shown by Izzo[34] from 2005. Analysis of this plot tells us which direction we should try to move at the encounter time. In this case, the asteroid is predicted to miss the Earth. Recall, though, that the b point is computed without considering the effect of Earth's gravity. If the b point were to lie inside the expanded Earth radius (dashed line), it means the real trajectory would be perturbed enough by Earth's gravity that it would actually hit Earth.

The goal is to move the asteroid so that its uncertainty ellipsoid avoids both Earth and the keyhole region. It is particularly interesting to note the direction of the asteroid's along-track velocity. For this encounter, it is oriented along the negative z-axis of the b-plane. For a given amount of fuel, the spacecraft can move the furthest in the along-track direction. This is also, however, the largest dimension of the uncertainty ellipsoid.

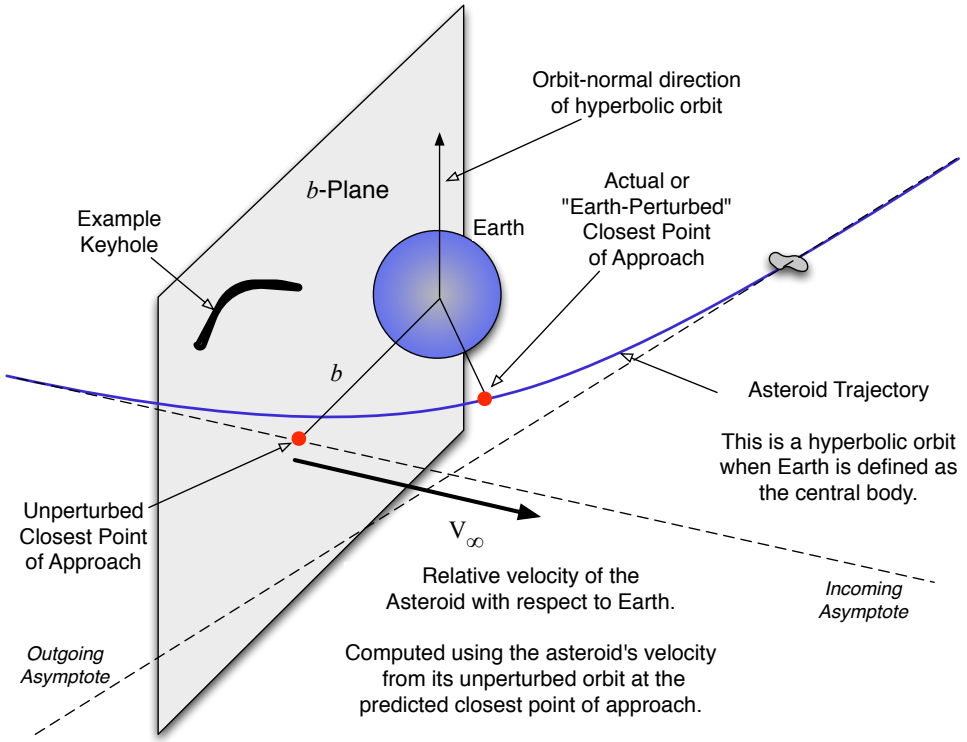

Figure 6. b-Plane Diagram. Illustrates the geometry of the encounter as the relative velocity vector intersects the b-Plane. The plane includes the line from Earth to the predicted closest point of approach, and it is perpendicular to the incoming asymptote.

For a given encounter, we should consider where the b point is with respect to Earth and the keyhole region, as well as the size of the uncertainty ellipsoid, and choose the best direction to maneuver.

6. Asteroid Deflection Maneuver

With several DFD engines attached to different places around the asteroid, we can apply thrust in any direction. For a given thrust T, the imparted acceleration over time is:

$$a(t) = \frac{T}{m_A + m_S(t)} = \frac{T}{m_A + m_S(0) - \dot{m} \times t} \tag{4}$$

where m_A is the asteroid mass, $m_S(t)$ is the time-varying spacecraft mass, and $\dot{m}$ is the mass flow rate. Because the mass of the spacecraft is negligible compared to the mass of the asteroid, this effectively gives us a constant mass system during the deflection maneuver. The magnitude of the acceleration is therefore just varied directly with the thrust, and may be expressed as:

$$a = \frac{T}{m_A} \tag{5}$$

With the DFD engine, the thrust is related to the exhaust velocity and power according to the equation:

$$T = \frac{2P\eta}{u_E} \tag{6}$$

This means that for a given power, we can achieve higher thrust at the expense of reduced exhaust velocity. Making this trade-off will increase the mass flow rate, though, since:

$$\dot{m} = \frac{T}{u_E} \tag{7}$$

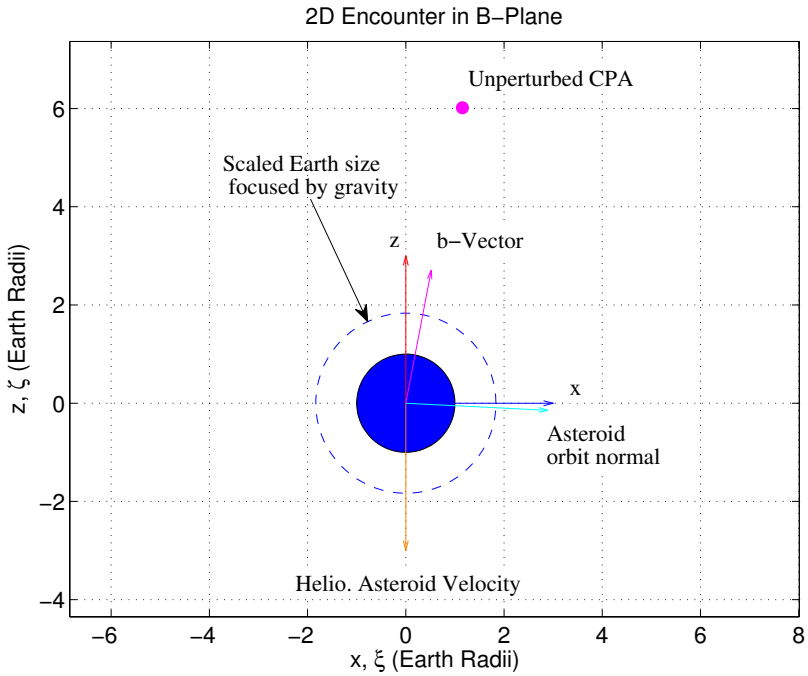

Figure 7. *b*-**Plane plot of the Earth-Apophis encounter in 2029.**

Using (6) to express u_E in terms of thrust and power, the mass flow rate expression becomes:

$$\dot{m} = \frac{T^2}{2P\eta} \tag{8}$$

This shows that while we can increase the thrust to impart higher accelerations, it causes the propellant to be consumed much more quickly.

To compute the deflection maneuver, we model the relative orbit dynamics of the asteroid using Gauss' variational equations (GVE).[35] The well-known GVE continuous-time dynamics relate the applied acceleration in a local reference frame to the instantaneous rate of change in the orbital elements.

We discretize the dynamics at a finite number of points along the trajectory using a zero-order hold sample. This allows us to create a discrete linear time-varying system that defines the orbital element differences $\delta\boldsymbol{e}$ over times $t_k \in [t_0, t_N]$ as a linear function of the applied accelerations $\boldsymbol{u}_k$. This approach has been used by Princeton Satellite Systems in several different types of formation flying and collision avoidance maneuver examples.[36–38]

It is instructive to consider two separate problems. In the first problem, we seek to maximize the separation distance at the time of impact, subject to a constraint on the total ΔV applied. This problem is formulated as follows:

Problem 1: Maximize Separation with Limited Delta V

$$\begin{aligned} &\text{Maximize} && \boldsymbol{q}^T \delta\boldsymbol{e} \\ &\text{Subject to} && \sum_{j=1}^{N} \left(|\boldsymbol{u}_j(1)| + |\boldsymbol{u}_j(2)| + |\boldsymbol{u}_j(3)|\right) \Delta T_j \leq \Delta V_{\max} \\ & && 0 \leq \tilde{\boldsymbol{u}} \leq u_{\max} \end{aligned} \tag{9}$$

where ΔT_j is the duration of the j^{th} time step, and the vector $\tilde{\boldsymbol{u}}$ is the stacked set of accelerations $\boldsymbol{u}_k$ over time points $k = 1, \ldots, N$. The vector $\boldsymbol{q}$ is the linear combination of orbital element differences that aligns the relative state in the desired spatial direction in the Hills coordinate frame. We choose the along-track direction as it permits the largest change in distance for a given amount of ΔV.

An alternate approach is to impose a minimum separation distance $d_{\min}$ at the time of impact, and meet that constraint in a way that minimizes the total ΔV applied. This approach can also take into account the initial state covariance C of the asteroid when defining the separation constraint. The new robust problem formulation is expressed as:

Problem 2: Minimize Delta V with Robust Avoidance Constraint

$$\begin{aligned} \text{Minimize} \quad & \sum_{j=1}^{N} \Delta T_j \left(|\boldsymbol{u}_j(1)| + |\boldsymbol{u}_j(2)| + |\boldsymbol{u}_j(3)| \right) \\ \text{Subject to} \quad & \boldsymbol{q}^T G_k \tilde{\boldsymbol{u}} \geq d_{\min} + \Delta d_{unc} \quad i = 1, \ldots, M \\ & 0 \leq \tilde{\boldsymbol{u}} \leq u_{\max} \end{aligned} \tag{10}$$

where $\Delta d_{\min} = ||\boldsymbol{q}^T H_N C||$ is computed as the worst-case realization of the initial state (with covariance C) in the direction of our avoidance constraint at the final point, $k = N$.

7. Analysis of Deflection Capability

We can use the optimal maneuver planning algorithms to gain some insight into the size and number of spacecraft needed to achieve a desired deflection. For a given maximum Delta-V and maximum thrust value, we compute the corresponding maximum separation distance that can be achieved as well as the mass of fuel consumed. Results for a Delta-V range of 0.1 to 1.0 m/s are displayed in Fig. 8. A similar plot is shown in Fig. 9 for a smaller Delta-V range of 0.01 to 0.1 m/s. Note that this is the Delta-V imparted to the asteroid, which is of course much smaller than the propulsion system Delta-V capability due to the large asteroid mass.

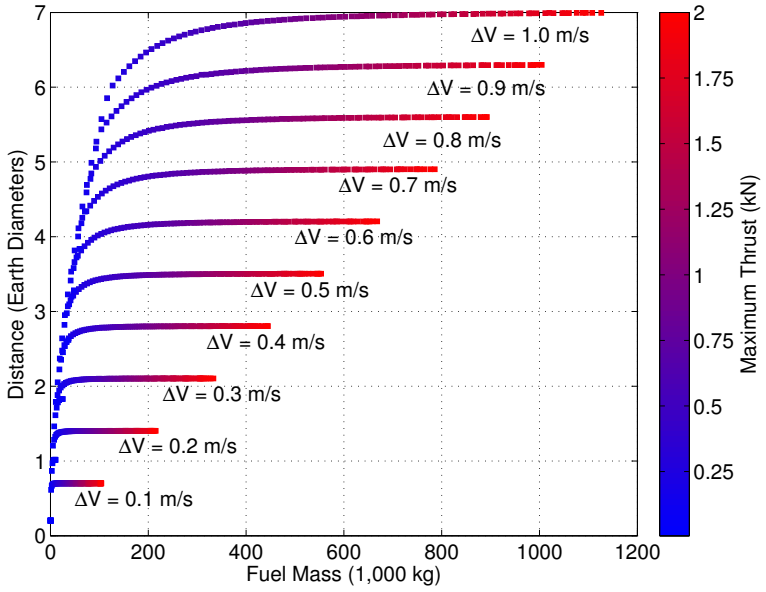

Figure 8. Separation distance achieved for a given fuel mass and thrust. This is applied to an Apophis-like orbit for an asteroid half the size of Apophis. The maneuver starts one year before the encounter.

Fig. 8 and 9 plot the relative distance achieved at the impact time against the required fuel mass. Each curve represents a different ΔV. The trends show that the separation distance increases monotonically with the fuel mass, as we would expect, but they also indicate a law of diminishing returns. Once the maximum thrust increases past about 0.5 kN, the increase in separation distance becomes negligible. This knee in the curve occurs at the same point for each ΔV value. This provides valuable insight, as it suggests a maximum thrust near 0.5 kN will provide the best performance for this deflection mission.

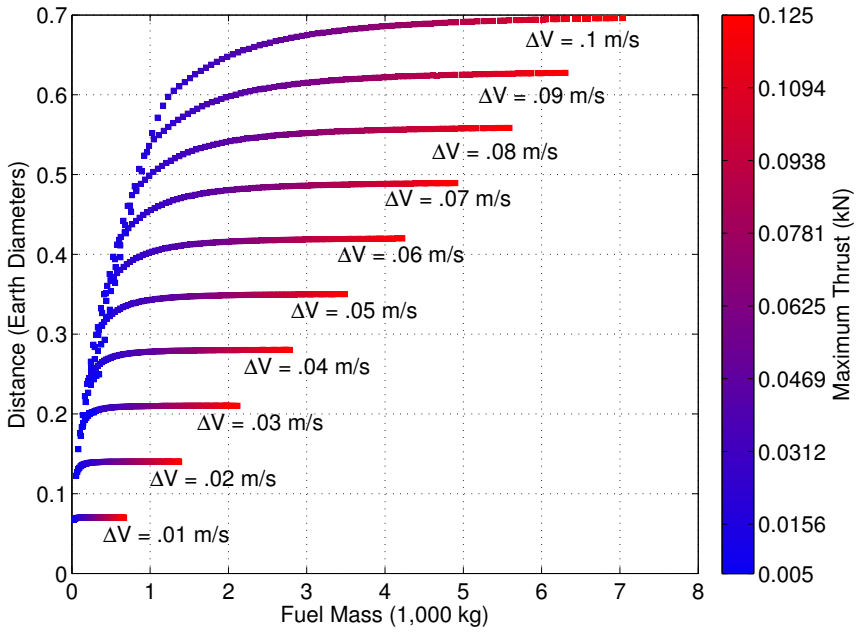

Figure 9. Separation distance achieved for a given fuel mass and thrust. This is the same analysis as shown in Figure 8 but over a smaller range of ΔV.

8. Earth Sphere of Influence

Another interesting aspect to consider is at what point during the approach does the gravitational effects of the Earth begin to take an important role in defining the Apophis trajectory. For the majority of the Apophis orbit considered, the gravitational acceleration due to the Sun is the primary influence on the orbital motion of the asteroid. Within some sphere of influence, the gravitational pull on Apophis from the Earth will exceed that of the Sun. At the time of impact, the gravitational acceleration imparted on Apophis by the Sun is approximately $5.89 \cdot 10^{-6}$ km/s^2. To have the same magnitude of acceleration from Earth's gravity, the asteroid would have to be 260,000 km away from Earth, or approximately 20 Earth diameters. By this point, the analysis should include Earth as the central body with the Sun gravitation force modeled as a perturbation. This is illustrated in Fig. 10.

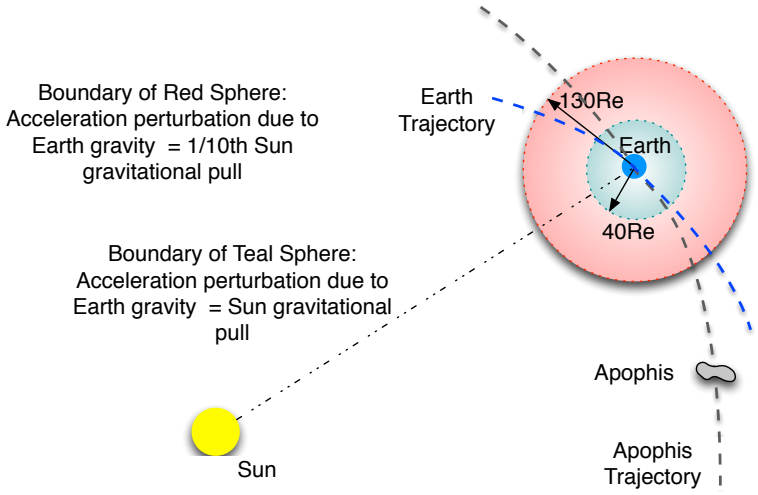

Figure 10. Earth Sphere of Influence relative to the Apophis trajectory

The relative velocity of Apophis with respect to the Earth at impact is 5.5 km/s and it takes 12.8 hours to go 20 Earth diameters at that speed. Thus, over the 365 days of the maneuver, only the last 1/2 day is the Earth close enough to dominate the gravitational acceleration. If we reduce the threshold to 1/10 that of sun's acceleration, the distance is 65 Earth diameters, which corresponds to the last 42 hours of the trajectory prior to impact.

5. Example Mission

The example mission is for an asteroid one-half the size Apophis. A CAD model of the asteroid is shown in Figure 11. Using this geometric representation of the asteroid surface, and assuming a uniform mass density, we have modeled the structure as a tetrahedral mesh to numerically compute the mass distribution and moment of inertia. The length of the asteroid is 160 m, and we find that the mass is 3.3737×10^9 kg.

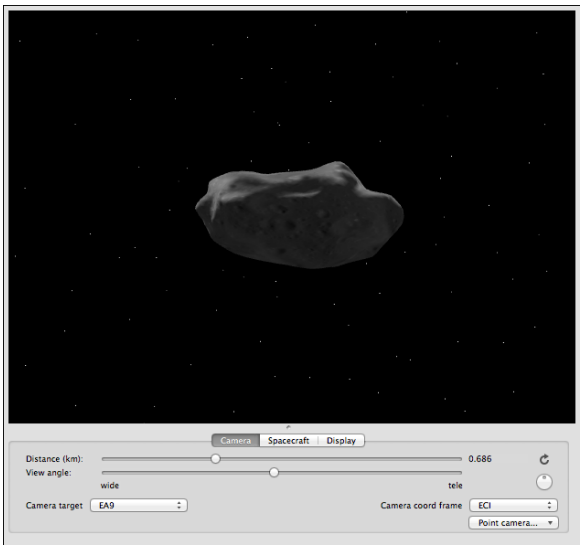

Figure 11. Apophis.

Since the asteroid is not predicted to hit the earth, we perturb it slightly in order to force an artificial collision. The osculating orbital elements of Apophis are computed from the JPL Horizons online service[b] for April 13, 2028 – one year prior to the close encounter. These are given in Table 2, along with the modified elements that produce a collision with Earth. The semi-major axis is in units of AU and the angles are in degrees.

Table 2. Orbital elements for Apophis and a modified set to force a collision.

	Semi-major axis	Inc.	Right Asc.	Arg. of Perigee	Eccentricity	Mean Anom.
Apophis	0.9224	3.835	203.858	126.738	0.1911	-153.782
Modified	0.9224	3.238	203.801	127.712	0.1804	-105.940

1. Maximize Separation

We first plan an avoidance maneuver according to Problem 1, maximizing the along-track distance at the time of impact. The goal is to move at least two Earth radii. The maneuver begins 365 days prior to the encounter, as in the previous analysis. Using Fig. 8 as a guide, we find 2 Earth radii on the vertical axis and find that a ΔV of 0.3 m/s is required. The knee of the curve is reached at about 0.5 kN, which we choose as our maximum thrust. We therefore set $\Delta V_{\max} = 3 \times 10^{-4}$ km/s and $u_{\max} = 0.5$ kN and solve Problem (9).

The optimal control history is shown in Fig. 12, along with the relative trajectory (about its nominal orbit) in the Hills coordinate frame. For this scenario, the optimal solution is to apply thrust purely in the

[b] http://ssd.jpl.nasa.gov/?horizons

along-track direction. As Fig. 12 shows, this occurs over a period of 23 days beginning on day 97 after the start of the maneuver. This time period is centered around the perigee of the asteroid's orbit, where it is most effective to generate along-track drift.

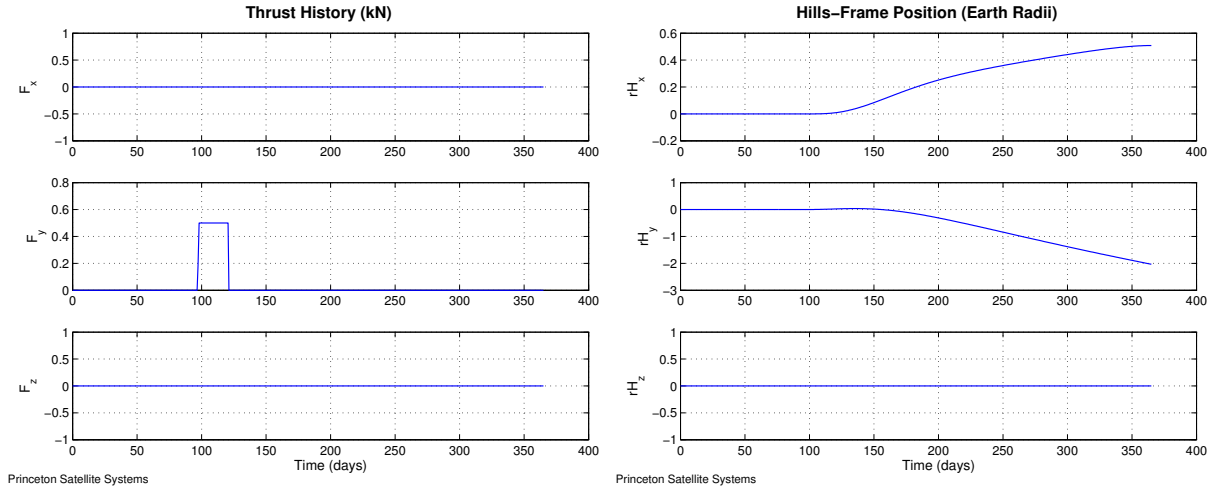

Figure 12. Optimal control and position history for the example deflection maneuver, Problem 1.

2. Minimize Delta-V with Directional Separation Constraints

We now plan a different avoidance maneuver, this time according to Problem 2. Again the maneuver begins 365 days prior to the encounter. In this case our objective is to minimize the total Delta-V consumed subject to the constraint that we achieve a desired separation distance along a given direction. Furthermore, we introduce the covariance associated with the initial state so that the constraint satisfaction is guaranteed to be robust to this bounded uncertainty. In this example we consider the original Earth-Apophis encounter in 2029, using the osculating orbital elements of Apophis that are obtained via JPL Horizons.

A plot of the b-plane encounter is shown in Fig. 13. The green circle represents the original, or unperturbed, closest point of approach (CPA). We apply an initial state uncertainty in the orbital element differences, where the semi-major axis error is $\pm 5,000$ km, and the remaining angles and eccentricity have an error of $\pm$1E-05. We perform a Monte Carlo simulation, generating random initial relative states within these bounds and then propagating forward to the encounter time to produce the red scatter plot. This clearly shows an elliptical region, which is equivalent to the projection of the covariance ellipsoid onto b-plane.

A simple rectangular keyhole region is used here for the sake of example. Of course, the true keyhole region would take on some other shape in this plane, but our approach works for any keyhole shape. Our goal is to plan the deflection maneuver so that the entire uncertainty ellipse avoids both the keyhole region and the Earth focus. For this particular geometry, we consider two alternate directions to move. The first option is to move along the vertical ζ axis, which as discussed before is primarily aligned with the asteroid's along-track axis. The second option is to move along the horizontal ξ axis, which is primarily along the asteroid's cross-track axis. In each case, the separation constraint is simply for the terminal relative state to lie on one particular side of the keyhole box. Additionally, the constraint formulation automatically accounts for the worst-case state uncertainty so that it is guaranteed to be satisfied for any set of orbital elements within these bounds.

As Fig. 13 shows, the asteroid will have to be moved about 1.5 Earth radii in ζ direction to avoid the keyhole, and about 2 Earth radii in the ξ direction. The Delta-V to move along ζ is just 0.15 m/s, compared to 3.0 m/s for a comparable distance in ξ. As expected it is much easier to move the asteroid in the along-track direction.

The optimal control and position histories associated with the ξ-direction maneuver (cross-track) are shown in Fig. 14. In this case, the optimal solution is to apply thrust purely in the $\pm$ cross-track direction at certain times in the orbit. As Fig. 14 shows, there are three periods of time where the thrust is applied. These periods occur over the first 25 days, then again from about day 75 to day 125, and once more from

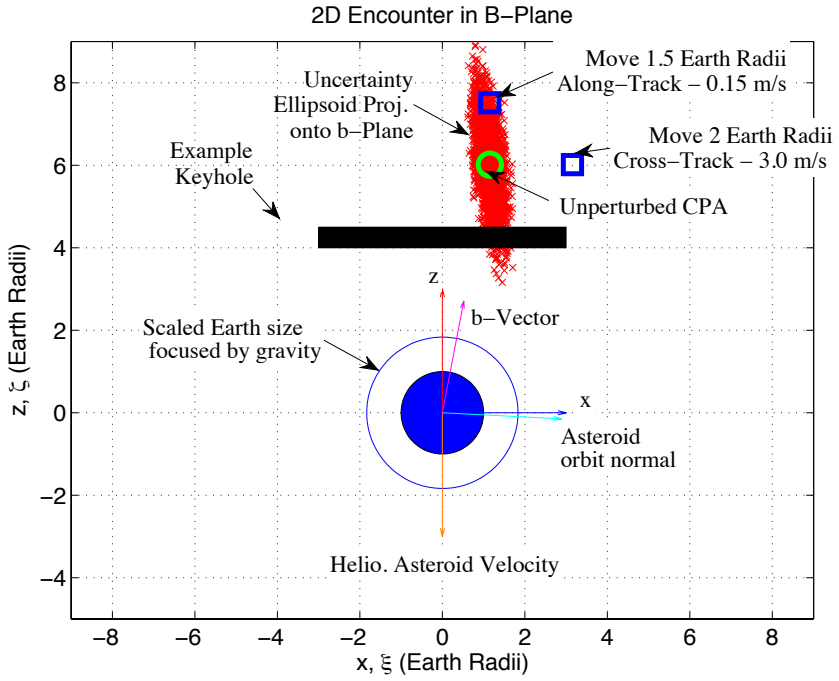

Figure 13. *b*-**Plane plot of the Earth-Apophis encounter in 2029 with an example keyhole. The red scatter plot illustrates the bounded region of** *b*-**plane intercept points subject to initial state covariance in the relative orbital elements 1-year prior to encounter.**

about day 200 to day 300. The timing and direction of the burns are chosen by the optimization such that the larges changes in inclination and right ascension are attained for a given Delta-V.

6. Conclusion

As we continue to study our near-Earth environment in space, we will continue to discover the presence of more and more asteroids. We know that, over time, large asteroid impacts have caused major climate changes, and smaller impacts have created tidal waves or destroyed large areas. Those that pose the biggest danger are easy to detect, while those that are too hard to find are typically too small to present a significant risk. However, there is a wide range of asteroid sizes (e.g. 30 m to 1 km) that are both too small to guarantee early detection, yet also large enough to incur major regional damage if they were hit Earth. This class of asteroid may be discovered too late to employ an ideal deflection mission, which requires advanced warning of several years.

In this paper, we have presented the Direct Fusion Drive (DFD) as a candidate future technology that could be used to deflect medium-size asteroids with just one year of warning. Under ongoing development at PPPL, the DFD design applies a field-reversed configuration (FRC) with several innovations to create a compact, light-weight engine that can yield high exhaust velocity with moderate thrust. The next test reactor, PFRC-3, will work at higher temperatures and pressures prior to the fourth test reactor that will achieve a burning plasma. Additional work is needed on low-mass neutron shielding, superconducting coils, refrigerators and heat engines that compose the balance of plant.

We examined the general geometry of asteroid encounters, and developed a maneuvering strategy that uses relative orbit dynamics in a model predictive framework in order to achieve desired relative position criteria at the encounter time. This approach used Gauss' variational equations to model the relative orbit dynamics and linearized the system at discrete points along the trajectory, allowing the maneuver problem to be posed as a high-dimensional linear program with terminal costs, control costs, and terminal constraints. Considering the 2029 Apophis encounter as an example, and using the DFD as our propulsion system, we developed optimal deflection maneuvers over a range of Delta-V budgets and considered a range of maximum thrust values to explore the trade space. Example maneuvers were presented that avoid both the Earth focus

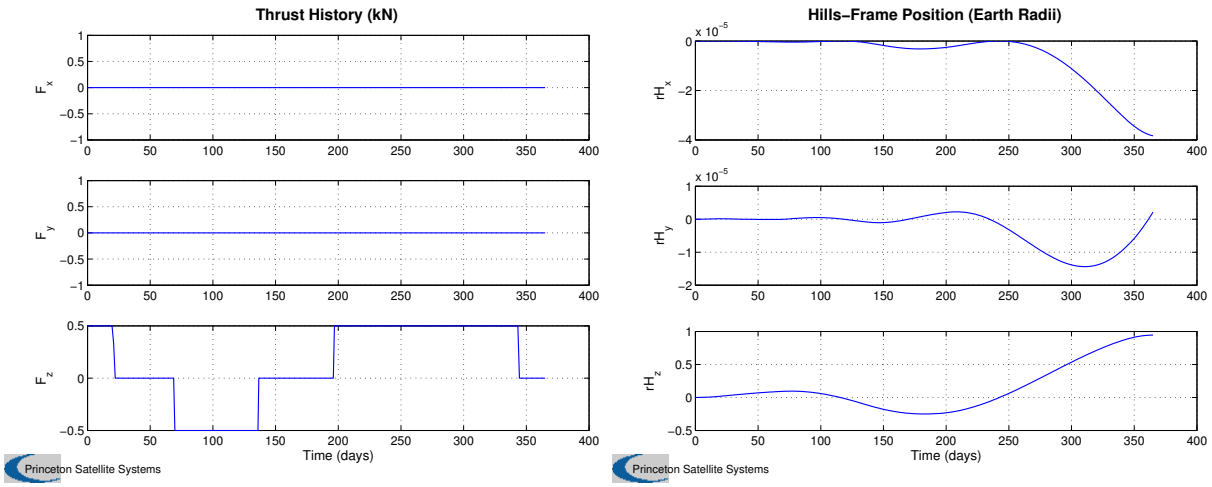

Figure 14. Optimal control history and position history for the example deflection maneuver, Problem 2.

and the keyhole region, and take into account initial state uncertainty so that the avoidance constraints are satisfied robustly.

Future work will be to examine the impact of state uncertainty and disturbances on the maneuver performance. Further design of the asteroid interface must also be performed, accounting for known and potential asteroid compositions. A system-level trade study should be undertaken to compare the effectiveness of our solid-mating approach to one that impinges the thrust plume on the asteroid without any physical attachment. Additional work on de-spinning strategies is also required.

Acknowledgments

We thank Dr. T. Kornack for calculations on energy extraction by RMF_o. This work was supported, in part, by DOE contract No. DE-AC02-09CH11466.

References

[1]Chapman, C. R., "The hazard of near-Earth asteroid impacts on earth," *Earth and Planetary Science Letters*, Vol. 222, No. 1, 2004, pp. 1 – 15.

[2]Merikallio, S. and Janhunen, P., "Moving an asteroid with electric solar wind sail," *Astrophysics and Space Sciences Transactions*, Vol. 6, No. 1, 2010, pp. 41–48.

[3]Edward T. Lu, S. G. L., "Gravitational tractor for towing asteroids," 2005.

[4]Pajer, G., Razin, Y., Paluszek, M., Glasser, A., and Cohen, S., "Modular Aneutronic Fusion Engine," *Space Propulsion 2012*, AAF-EAS-CNES, 2012.

[5]Razin, Y., Paluszek, M., Ham, E., Pajer, G., Mueller, J., Cohen, S., and Glasser, A. H., "Compact Aneutronic Fusion Engine," *International Astronautical Congress,*, Naples, Italy, October 2012.

[6]Paluszek, M., Hurley, S., Pajer, G., Thomas, S., Mueller, J., Cohen, S., and Welch, D., "Modular Aneutronic Fusion Engine for an Alpha Centauri Mission," *DARPA 100 Year Starship Conference*, Orlando, Florida, September 2011.

[7]Cohen, S. and Liu, C., "Private Communication," .

[8]Rider, T., "Fundamental Limitations on Plasma Fusion Systems Not in Thermodynamic Equilibrium," *Physics of Plasmas*, Vol. 4, 1997, pp. 1039.

[9]Myers, C. E., Edwards, M. R., Berlinger, B., Brooks, A., and Cohen, S. A., "Passive Superconducting Flux Conservers for Rotating-Magnetic-Field Driven Field-Reversed Configurations," *Fusion Science and Technology*, Vol. 61, No. 4587, January 2012, pp. 86.

[10]Chopra, O. K., "Degradation of LWR Core Internal Materials due to Neutron Irradiation," Tech. Rep. NUREG/CR-7027, Argonne National Laboratory, December 2010.

[11]Dawson, J., *Advanced Fusion Reactors*, Vol. B, Academic Press, New York, 1981, p. 453.

[12]Cohen, S., "A Fusion Power Plant Without Plasma-Material Interactions," Tech. Rep. PPPL-3245, Princeton Plasma Physics Laboratory, September 1997.

[13]Arefiev, A. V. and Breizman, B. N., "MHD Scenario of Plasma Detachment in a Magnetic Nozzle," Tech. rep., Institute for Fusion Studies, The University of Texas, July 2004.

[14]Tarditi, A. G. and Steinhauer, L. C., "Plasma Flow Control in a Magnetic Nozzle for Electric Propulsion and Fusion Scrape-Off Layer Applications," No. 2C31, 2011 International Sherwood Fusion Theory Conference, November 2011.

[15]Cohen, S., Sun, X., Ferraro, N., Scime, E., Miah, M., Stange, S., Siefert, N., and Boivin, R., "On Collisionless Ion and Electron Populations in the Magnetic Nozzle Experiment (MNX)," *IEEE Transactions on Plasma Science*, Vol. 34, No. 3, june 2006, pp. 792–803.

[16]Martinez, M. M., "On Plasma Detachment in Propulsive Magnetic Nozzles," *Physics of Plasmas*, Vol. 18, No. 035504, 2011.

[17]Santarius, J. F., "Lunar ^{3}He, Fusion Propulsion, and Space Development," *Lunar Bases and Space Activities of the 21st Century*, edited by W. W. Mendell, J. W. Alred, L. S. Bell, M. J. Cintala, T. M. Crabb, R. H. Durrett, B. R. Finney, H. A. Franklin, J. R. French, & J. S. Greenberg, Sept. 1992, pp. 75–81.

[18]Cheong, M. C., "Analysis of Heat and Particle Flows in the Scrape-Off Layer of a Field-Reversed Configuration," 2012 Internship Program, Program in Plasma Science & Technology, PPPL.

[19]Binderbauer, M., Guo, H. Y., M.Tuszewski, Putvinski, S., Sevier, L., and Barnes, D., "Dynamic Formation of a Hot Field Reversed Configuration with Improved Confinement by Supersonic Merging of Two Colliding High-Compact Toroids," *Physical Review Letters*, Vol. 105, 2010, pp. 045003.

[20]Tuszewski, M., Smirnov, A., and Thompson, M., "Field Reversed Configuration Experiment Through Edge-Biasing and Neutral Beam Injection," *Physical Review Letters*, Vol. 108, No. 255008, June 2012.

[21]Wesson, J., *Tokamaks*, Oxford Univ. Press, Oxford, 3rd ed., 2004.

[22]Cohen, S. A., Berlinger, B., Brunkhorst, C., Brooks, A., Ferarro, N., Lundberg, D., Roach, A., and Glasser, A., "Formation of Collisionless High-β Plasmas by Odd-Parity Rotating Magnetic Fields," *Physical Review Letters*, Vol. 98, 2007, pp. 145002.

[23]Rosenbluth, M. N. and Bussac, M. N., "MHD Stability of Spheromak," *Nuclear Fusion*, Vol. 19, 1978, pp. 489.

[24]Glasser, A. and Cohen, S. A., "Ion and Electron Acceleration in the Field-Reversed Configuration with an Odd-Parity Rotating Magnetic Field," *Physics of Plasmas*, 2002, pp. 2093–2102.

[25]Landsman, A. S., Cohen, S. A., and Glasser, A., "Onset and Saturation of Ion Heating by Odd-Parity Rotating Magnetic Fields in an FRC," *Physical Review Letters*, Vol. 96, 2006, pp. 015002.

[26]Cohen, S. A., Landsman, A. S., and Glasser, A., "Stochastic Ion Heating in a Field-Reversed Configuration Geometry by Rotating Magnetic Fields," *Physics of Plasmas*, Vol. 14, 2007, pp. 072508.

[27]TEKNA, "1 MW Industrial Unit," 2012.

[28]Chapman, C., "The Hazard of Near-Earth Asteroid Impacts on Earth," *Earth and Planetary Science Letters*, Vol. 222, 2004.

[29]Hills, J. and Goda, M., "Damage from Comet-Asteroid Impacts with Earth," *Phyisca D*, Vol. 133, 1999.

[30]Garshnek, V., Morrision, D., and Jr., F. B., "The Mitigation, Management, and Survivability of Asteroid/Comet Impact with Earth," *Space Policy*, Vol. 16, 2000.

[31]Ryan, W. and Ryan, E., "Rotation Rates of Recently Discovered Small Near-Earth Asteroids," *Advanced Maui Optical and Space Surveillance Technologies Conference*, 2009.

[32]Mueller, J., Paluszek, M., Thomas, S., Knutson, A., Klein, D., and Tam, M., "Asteroid Prospector," *27th Annual AIAA/USU Conference on Small Satellites*, August 2013.

[33]Scheeres, D. and Schweickart, R., *The Mechanics of Moving Asteroids*, American Institute of Aeronautics and Astronautics, 2013/09/16 2004.

[34]Izzo, D., Bourdoux, A., Walker, R., and Ongaro, F., "Optimal trajectories for the impulsive deflection of near earth objects," *Acta Astronautica*, Vol. 59, No. 1, 2006, pp. 294–300.

[35]Breger, L. and How, J., "GVE-Based Dynamics and Control for Formation Flying Spacecraft," *2nd International Symposium on Formation Flying Missions and Technologies*, NASA Goddard Space Flight Center, Washington, D.C., 2004.

[36]Mueller, J. B. and Larsson, R., "Collision Avoidance Maneuver Planning with Robust Optimization," *7th International ESA Conference on Guidance, Navigation and Control Systems*, June 2008.

[37]Mueller, J., "Onboard Planning of Collision Avoidance Maneuvers Using Robust Optimization," *AIAA InfoTech@Aerospace Conference*, No. AIAA-2009-2051, Seattle, WA, April 2009.

[38]Mueller, J., Griesemer, P., and Thomas, S., "Avoidance Maneuver Planning Incorporating Station-Keeping Constraints and Automatic Relaxation," *Journal of Aerospace Information Systems*, Vol. 10, No. 6, 2013, pp. 306–322.